RSC Advances

This is an *Accepted Manuscript*, which has been through the Royal Society of Chemistry peer review process and has been accepted for publication.

Accepted Manuscripts are published online shortly after acceptance, before technical editing, formatting and proof reading. Using this free service, authors can make their results available to the community, in citable form, before we publish the edited article. This *Accepted Manuscript* will be replaced by the edited, formatted and paginated article as soon as this is available.

You can find more information about *Accepted Manuscripts* in the Information for Authors.

Please note that technical editing may introduce minor changes to the text and/or graphics, which may alter content. The journal's standard Terms & Conditions and the Ethical guidelines still apply. In no event shall the Royal Society of Chemistry be held responsible for any errors or omissions in this *Accepted Manuscript* or any consequences arising from the use of any information it contains.

ROYAL SOCIETY OF CHEMISTRY

www.rsc.org/advances

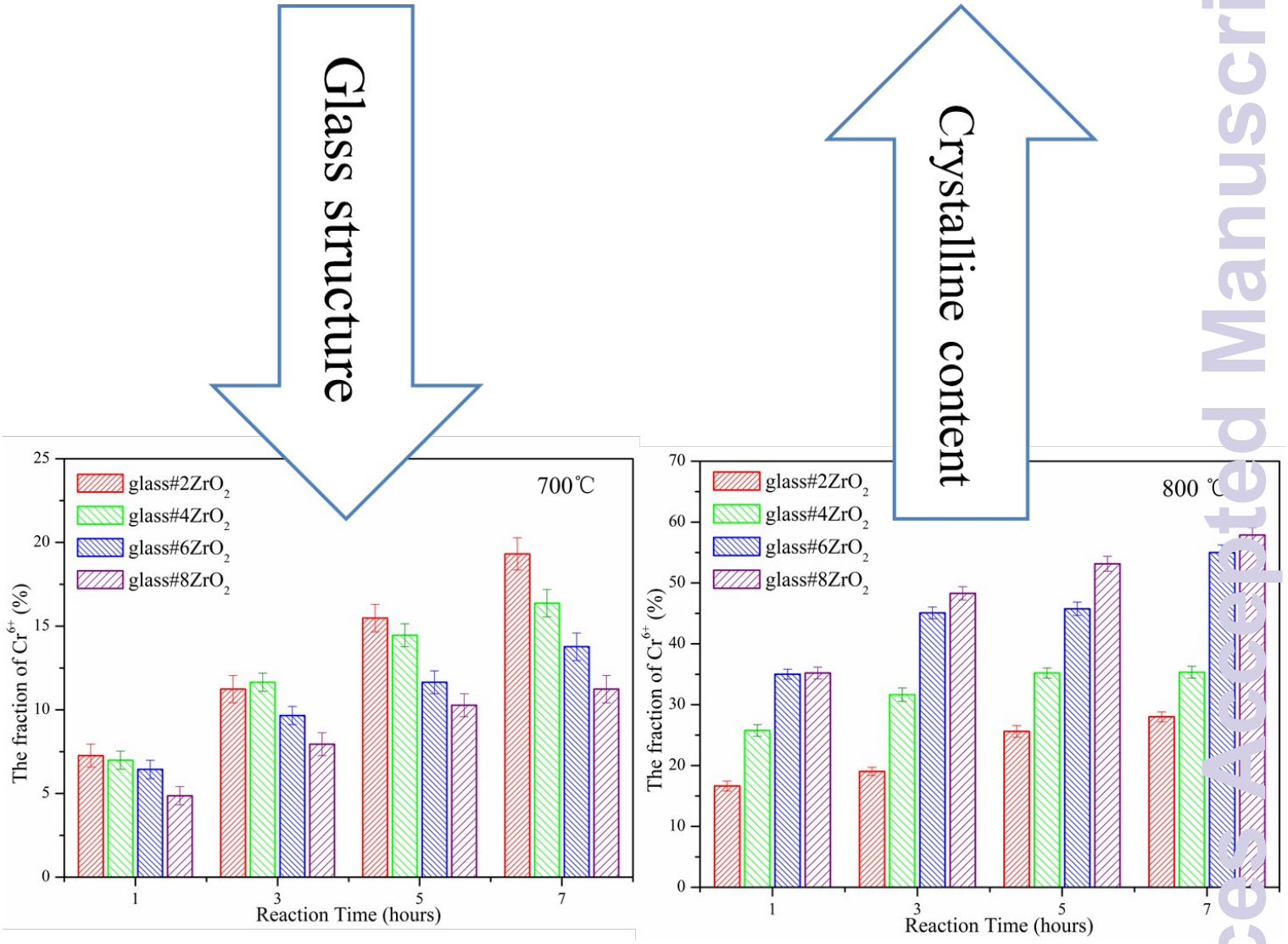

The fraction of Cr^{6+} in the glass/Cr_2O_3 reaction couple decreases significantly with increasing ZrO_2 content at 700 ℃ because of the condensed glass structure; whereas, the fraction of Cr^{6+} increases with increasing ZrO_2 content at 750 and 800 ℃, due to the increase in residual glass content in the glass-ceramics.

RSC Advances Accepted Manuscript

Development of the $CaO–SrO–ZrO_2–B_2O_3–SiO_2$ Sealing Glasses for Solid Oxide Fuel Cell Applications: Structure-Property Correlation

Qi Zhang[1], Hsiwen Yang[2], Fanrong Zeng[3], Shaorong Wang[3], Dian Tang[1] and Teng Zhang*[,1]
[1]College of Materials Science and Engineering, Fuzhou University, Fuzhou, Fujian 350108, China
[2]Department of Materials Science and Engineering, National United University, Miao-Li 36003, Taiwan, China
[3] CAS Key Laboratory of Materials for Energy Conversion, Shanghai Institute of Ceramics, Chinese Academy of Sciences (SICCAS), 1295 Dingxi Road, Shanghai 200050, China

In this study, the structure-property correlation in the $CaO–SrO–ZrO_2–B_2O_3–SiO_2$ sealing system is systematically investigated. In particular, the effect of ZrO_2 on the structure and chemical compatibility of the glasses is clearly demonstrated. The increases in the glass transition temperature and softening temperature of the glasses indicate that the glass structure is condensed by the ZrO_2 dopant, which is further confirmed by the ^{11}B and ^{29}Si NMR spectra. Furthermore, the addition of ZrO_2 reduces the crystallization tendency of the glasses. The fraction of Cr^{6+} in the glass/Cr_2O_3 reaction couple decreases significantly with increasing ZrO_2 content at 700 ºC because of the condensed glass structure, whereas the fraction of Cr^{6+} increases with increasing ZrO_2 content at 750 and 800 ºC. This behavior is related to the increase in residual glass content in the glass-ceramics. Good bondage can be observed at the interfaces between glasses and Crofer 22APU after held at 800 ºC for 500 hours. These results demonstrate the suitability of the Zr-containing glass-ceramics as sealing materials for SOFC applications.

Key Words: Solid Oxide Fuel Cells; Interfacial Reaction; Sealing Glass; Glass Structure; Crystalline Structure

* Corresponding author. Tel.: +86 591 22866540; fax: +86 591 22866537.
E-mail address: teng_zhang@fzu.edu.cn (T. Zhang).

RSC Advances Accepted Manuscript

1. Introduction

Solid oxide fuel cells (SOFCs) are attractive electrochemical devices that convert chemical energy into electricity with great efficiency.[1-4] As a key component of SOFCs, the sealing glass has to meet certain requirements for its electrical resistivity,[5-7] thermal stability,[8-14] and chemical compatibility.[15-17]

Interactions between glass-ceramic sealants and ferritic interconnects at the SOFC operational temperatures have been found to result in the formation of interfacial phases potentially detrimental to the performance of the SOFC stacks.[18-21] Alkali ions or residual water in some glass compositions significantly increase the vaporization of chromium from the interconnects.[18, 22] The transport of Cr-vapors, as CrO_3 or $CrO_2(OH)_2$, can lead to the formation of alkaline earth chromates on glass surfaces well-removed from the glass-metal interface.[22] The high coefficients of thermal expansion (CTEs) of these chromates, *e.g.,* $BaCrO_4$ and $SrCrO_4$ (~18 to 20×10^{-6}/K),[23] contributes to the physical separation of the sealing glass (CTE~12.5×10^{-6}/K) and the interconnect (~13×10^{-6}/K) because of the large CTE differences, and leads to significant losses in bond strength between SOFC glasses and interconnect materials.[24]

It has been reported that the extent and nature of the reactions between glass sealants and different types of alloys depend on the alloy compositions and the exposure conditions.[19, 22] For chromia–forming alloys, the edges of the seals where oxygen or air is accessible typically exhibit $BaCrO_4$ formation. For a more oxidation resistant alloy, *e.g.*, a Ni-based super alloy, the extent of the formation of $BaCrO_4$ can be limited. The addition of aluminum to the interconnect alloy can suppress the formation of interfacial chromates and so lead to stronger glass-metal seals.[25] Likewise, the addition of protective coatings to the interconnects has been used to

RSC Advances Accepted Manuscript

suppress chromate formation,[26] but often at the cost of conductivity. Compared with the great efforts made to modify the interconnects,[27-30] few works have been done to improve the chemical compatibility of sealing glass because of the difficulty of quantitative investigation of the glass/metal interaction in the complex SOFC stack.[31-33]

On the other hand, the design of compliant seals has attracted increasing attention in recent years. Ideally, the glass should remain viscous at high temperature, *i.e.,* 700-800 °C, to release the thermal stress generated by any mismatch in the coefficient of thermal expansion (CTE) during thermal cycling. The glass melt should also be able to flow to heal any cracks in the seals that form during operation, while still maintaining the necessary mechanical strength to support the substrates. The key of this design is to have sufficient amount of residual glass under the operational condition of SOFC. However, our recent work has revealed that alkaline earth ions (Sr^{2+}) can react with a Cr-containing interconnect to form a detrimental chromate phase, *e.g.*, $SrCrO_4$, much more easily in the glass matrix than they can in crystalline phases.[34] Therefore, chemical compatibility is of great importance for fabricating compliant seals.

It is known that ZrO_2 generally reduces the crystallization tendency of glasses and thus constitutes a representative model system to investigate the chemical compatibility of compliant seals. In this paper, ZrO_2 was added gradually (from 2 to 8 mol. %) into the SrO-CaO-SiO_2-B_2O_3 sealing glass system (hereafter, these samples are called glass#2ZrO_2 and glass#8ZrO_2, respectively). Attention was focused on the following questions: (1) How does ZrO_2 affect the structures of glasses and glass-ceramics? (2) How does ZrO_2 affect the thermal and electrical properties of glasses? (3) How does ZrO_2 affect the interfacial reaction between sealing glasses and

RSC Advances Accepted Manuscript

Cr-containing interconnects? In particular, the reaction temperature was chosen to be 700, 750, or 800 ºC to clarify the structural dependence of the interfacial reaction.

2. Experimental

2.1 Preparation of glasses and glass-ceramics

Glasses from the CaO-SrO-B_2O_3-SiO_2-ZrO_2 system were melted in a Pt-crucible in air at 1500 ºC for one hour. The nominal compositions of the glasses (mol. %) are shown in Table 1. Some of the melt was poured into a stainless steel mold to obtain cylindrical glass specimens (25 mm length and 6 mm diameter), and the rest of the melt was quenched on a steel plate to form the glass. Glass powders were then crushed and sieved to a particle size of 45 to 53 μm. Pellets (10 mm diameter and 2 mm thickness) were obtained after uniaxial pressing of glass powders and were held at 700 and 800 ºC for up to 500 hours in air (referred to as 'glass-ceramics').

In recent years, there is a need to reduce the operational temperature from 900-1000 ºC for traditional SOFC into the so-called intermediate temperature (IT) range of 500–750 ºC, in order to reduce the corrosion rate of SOFC components.[35] Thus, most of sealing glasses are designed to be operated at the temperature range of 700-750 ºC, including the ZrO_2-containing glasses in present work.

It is known that long-term stability (static state) and thermal-cycling stability (dynamic state) are critical for sealing glasses. Many works on the sealing materials have been performed in static state in literature.[20, 21, 36-38] Therefore, the test scenarios in preset work are chosen to be at 800 ºC for 500 hours to accelerate the evolution of glass-ceramics as well as the glass-metal interface, which provides useful information on the long stability of sealing glasses. This will need a much longer time if testing at a low temperature (*e.g.*, 700 ºC).

RSC Advances Accepted Manuscript

2.2 Characterization of glass structure and crystalline structure of glass-ceramics

^{29}Si and ^{11}B magic-angle spinning (MAS) nuclear magnetic resonance (NMR) spectra were recorded for all quenched glasses. The spectra were acquired on a Bruker DSX-400MHZ spectrometer operating at a B_0 field of 9.4 T with ^{29}Si and ^{11}B Larmor frequencies of 79.5 and 128.4 MHz, respectively. The detailed procedure for the NMR measurement has been reported elsewhere.[39]

In addition, the crystalline phases in the glass-ceramic powders were identified by X-ray diffraction (XDS 2000, Scintag, Inc.). The crystalline content (wt. %) in the glass-ceramics that were held at 800 ºC for 2 hours was then calculated by the RIQAS software (Release 4.0.0.8, Materials Data, Inc., CA). The detailed procedure for the calculation has been described elsewhere.[40, 41]

2.3 Characterization of thermal and electrical properties of glasses

The onset crystallization temperature (T_x) of the glass powders was determined by performing differential scanning calorimetry (SDTQ600, TA, Inc.) at a heating rate of 10 ºC·min^{-1}. The thermal characteristics of the quenched glasses, including the CTE (between 200 and 600 ºC), glass transition temperature (T_g), and softening temperature (T_d), were determined by operating a dilatometer (DIL402C, NETZSCH, Inc.) at 10 ºC·min^{-1} in air. Glass-ceramics held at 800 ºC for 500 hours were also subjected to dilatometric measurements for comparison. The thermal properties of the quenched glasses and glass-ceramics are summarized in Table 2. The density of the quenched glasses was measured using the Archimedes method in water.

The electrical conductivity of the quenched glasses and glass-ceramics was measured in air from 650 to 750 ºC using a high resistance meter (4339B, Agilent,

RSC Advances Accepted Manuscript

Inc.). The measurement was performed with Pt current collectors and Pt wire, at a heating rate of 5 ºC·min^{-1}.

2.4 Characterization of interfacial reaction

Based on the previous experience in our lab, the adhesion test, such as pin-pull test, is hard to distinguish the adhesion strength between glass and metallic interconnect. First of all, the broken point often exists in the fragile glass instead of interface. In addition, the measured strength will be very close within experimental uncertainty if the reaction zone of different specimens has a similar thickness. Therefore, we propose a more reliable and sensitive approach for evaluating the interfacial reaction between sealing glass and Cr-containing interconnect, which is the main point of present work.

A ~20 mg mixture of glass and 10 wt. % Cr_2O_3 powders was reacted in an alumina boat in air for different times at 700, 750, or 800 ºC. After the reaction, the mixture was dissolved into ~200 ml of room-temperature deionized water, and the UV-VIS absorption spectra were recorded using an Optima 2000 DV (Perkin Elmer, Inc.). The concentration of Cr^{6+} in each solution was calculated by fitting the corresponding absorbance from the calibration curve derived from the K_2CrO_4 solutions. Three samples were made under identical conditions and were analyzed to determine the experimental uncertainty. The detailed procedure for this measurement has also been discussed elsewhere.[34, 42, 43]

In addition, the glasses were bonded to Crofer 22APU substrates and the interfacial reactions were characterized. The coated samples were held in air at 800 ºC for 500 hours. The glass/metal sealing couples were polished using SiC paper and an alumina suspension, as discussed elsewhere.[42] The polished samples were analyzed using field emission scanning electron microscopy (Supra-55, Zeiss, Inc.) and X-ray

RSC Advances Accepted Manuscript

energy dispersive analysis (EDS, X-Max, OXFORD instruments, Inc.). Sealing glasses were coated on only one side of the Crofer in present work, as reported by many colleagues in literature.[20, 21, 38, 44, 45] This fixture may not be a true representation of the interfacial chromate formation.

3. Results and discussion

3.1 Glass structure and crystalline structure of glass-ceramics

Fig. 1a shows the ^{11}B MAS NMR spectra of the glasses. The peak centers at -20 ppm can be assigned to BO_4 (four-fold coordinated boron species), whereas the peaks positioned at -9 and -14 ppm correspond to BO_3 (three-fold coordinated boron species).[46] The ratio of BO_3 to BO_4 increases with increasing ZrO_2 content, which reveals that a $BO_4 \rightarrow BO_3$ transition occurs in the glasses upon the addition of ZrO_2.

In addition, a single broad resonance peak positioned at approximately -80 ppm, corresponding mainly to Q^2 and Q^3 units, can be observed in the ^{29}Si MAS NMR spectra of the glasses, as shown in Fig. 1b. The chemical shift of ^{29}Si from -79 ppm for glass#2ZrO_2 to -78 ppm for glass#8ZrO_2 indicates an increasing densification degree of [SiO_4] tetrahedral with increasing ZrO_2 content.[39] Therefore, the addition of ZrO_2 strengthens the glass structure in present work, consistent with the previous results in literature.[47]

Fig. 2 shows the XRD patterns of glass-ceramics held at different temperatures. All species remain in an amorphous state after being held at 700 ºC for 5 hours, as shown in Fig. 2a. Shown in Fig.2b and Fig.2c are the XRD patterns of glass-ceramics held at 800 ºC for 2 and 500 hours, respectively. The patterns have been normalized by the intensity of the strongest peak ($2\theta = 31.2°$). Sr_2SiO_4 (ICDD Card No. 76-1494), $CaSiO_3$ (ICDD Card No. 43-1460), CaB_4O_7 (ICDD Card No. 83-2025) and $(Ca_{0.612}Sr_{0.388})ZrO_3$ (ICDD Card No. 89-8016) are the main phases in the

RSC Advances Accepted Manuscript

glass-ceramics. The standard diffraction pattern of $(Ca_{0.612}Sr_{0.338})ZrO_3$ (89-8016) has also been included at the bottom of Fig.2c for comparison. It is clear that most of the diffraction peaks corresponding for $(Ca_{0.612}Sr_{0.338})ZrO_3$ phase match the measured patterns very well.

To clarify the change in the diffraction peaks, the XRD patterns in Fig.2c have also been plotted in the 2θ range of 20-35°, as shown in Fig.2d. It is clear that the diffraction intensity of (400) plane in $CaSiO_3$ (2θ = 23.1°) increases when the ZrO_2 content increases from 2 to 8 mol. %, indicating the increasing $CaSiO_3$ content in glass-ceramics with the addition of ZrO_2. It is also worth noting that the intensity of (004) plane in $(Ca_{0.612}Sr_{0.388})ZrO_3$ (2θ = 30.9°) increases with increasing ZrO_2 content. This implies that the crystallization of $(Ca_{0.612}Sr_{0.388})ZrO_3$ in glass-ceramics can be facilitated by ZrO_2 dopant.

3.2 Thermal and electrical properties of glasses and glass-ceramics

The thermal properties of sealing glasses and glass-ceramics are summarized in Table 2. The glass transition temperature (T_g) increases from 685±3 to 726±3 ºC when the ZrO_2 content increases from 2 to 8 mol. % . In addition, the softening temperature (T_d) increases from 748±3 ºC for glass#2ZrO_2 to 787±3 ºC for glass#8ZrO_2. It has been found that increases in the glass transition temperature and softening temperature often indicate condensation of the glass network.[48] Considering the increases in the glass transition temperature and the softening temperature due to the ZrO_2 dopant observed in present work, it can be concluded that the Si-O bonding plays a predominant role in the overall glass structure and therefore results in condensation of the glass network.

Although this trend does not hold for glass#4ZrO_2 (4 mol. % ZrO_2), the onset crystallization temperature (T_x) of the sealing glasses increases from 869±3 ºC for

RSC Advances Accepted Manuscript

glass#2ZrO_2 to 901±3 ºC for glass#8ZrO_2. The temperature window between the T_d (or T_{MS}, the maximum shrinkage temperature) and T_x of sealing glasses, referred to as ΔT, is often considered an important criterion for evaluating their sealing behavior.[39] These ΔT values of the glasses with ZrO_2 dopants in the present work were high (from 114 to 157 ºC), indicating that these samples exhibit better sealing behavior than ZrO_2-free glass (823 - 739 = 84 ºC).[49]

Moreover, the crystalline content of the glass-ceramics held at 800 ºC for 2 hours decreases from 71±5 wt. % for glass#2ZrO_2 to 60±5 wt. % for glass#8ZrO_2. The increasing residual glass content in the glass-ceramics indicates that the addition of ZrO_2 reduces the tendency of the glasses to crystallize, due to the condensed glass network (in Fig.1 and Table 2). It is known that the addition of ZrO_2 can strengthen the glass network of borosilicate glasses and promote the formation of Q^2 structural units, which is consistent with the experimental results in present work. [39, 50, 51] The strengthened glass network reduces the crystallization tendency of glasses and results in the decrease in crystalline content of glass-ceramics held at 800 ºC for 2h (in Table 2).

It has also been reported that ZrO_2 conduced a-quartz-like structure in borosilicate glasses, which thus promoted a-quartz crystallization upon subsequent heat-treatment.[52] Therefore, one can deduce that ZrO_2 favors the formation of Q^2 structural units in glass network (in Fig.1b) and consequently facilitates the crystallization of Q^2-type species, *i.e.*, $CaSiO_3$,[53] after long-term heat-treatment in present work (in Fig.2c and Fig.2d).

The CTEs of the quenched glass#2ZrO_2, glass#4ZrO_2, glass#6ZrO_2, and glass#8ZrO_2 samples are 12.6, 13.1, 12.1, and 12.4 $\times 10^{-6}$ K^{-1}, respectively. The change in the CTE of the quenched glasses seems to be unrelated to the ZrO_2 content

RSC Advances Accepted Manuscript

and might be affected by technical factors such as the formation of pores in the glass cylinders during the pouring process. In contrast, it is clear that the CTE of the glass-ceramics held at 800 ºC for 500 hours, decreases from 12.2×10^{-6} K^{-1} for glass#2ZrO_2 to 10.5×10^{-6} K^{-1} for glass#8ZrO_2. The decrease in CTE can be related to the increasing $CaSiO_3$ content in glass-ceramics (in Fig.2c), because of its low CTE (9.4×10^{-6} K^{-1}).[54] It is also worth noting that the CTEs of the glasses and glass-ceramics are almost within the design range for SOFC sealing applications (*e.g.*, 11-13$\times10^{-6}$ K^{-1}).[1]

Fig.3 shows the temperature dependence of conductivity (log σ versus 1000 T^{-1}) for glasses and glass-ceramics, measured in air from 650 to 750 ºC. The conductivity for glass#2ZrO_2 and glass#8ZrO_2 is chosen for simplicity. It is clear that the conductivity (σ) of all species increases with increasing temperature, indicating the predominant role of ionic conductivity in present work. In addition, the conductivity of quenched glasses at each temperature decreases with ZrO_2 dopant. For example, the conductivity of glasses at 750 ºC decreases from 8.5×10^{-7} $S\cdot cm^{-1}$ for glass#2ZrO_2 to 5.6×10^{-7} $S\cdot cm^{-1}$ for glass#8ZrO_2. The decrease in conductivity of glasses with increasing ZrO_2 content further confirms the densification of glass network by ZrO_2 dopant in present work. It is worth noting that the conductivity of glass-ceramics held at 800 ºC for 500 hours increases with ZrO_2 dopant. For example, the conductivity of glass-ceramics at 750 ºC increases from 2.0×10^{-8} $S\cdot cm^{-1}$ for glass#2ZrO_2 to 2.4×10^{-7} $S\cdot cm^{-1}$ for glass#8ZrO_2. It has been reported that the conductivity of $CaZrO_3$ at 750 ºC is about 5.6×10^{-5} $S\cdot cm^{-1}$.[55] Considering the similar perovskite structure of $(Ca_{0.612}Sr_{0.388})ZrO_3$ and $CaZrO_3$, one can deduce that the increase in conductivity of

RSC Advances Accepted Manuscript

glass-ceramics relates to the increasing $(Ca_{0.612}Sr_{0.388})ZrO_3$ content with ZrO_2 dopant (in Fig.2d). On the other hand, we have also analyzed the residual glass in glass-ceramics by EDS. The results show that no zirconia can be detected in residual glass, which excludes the effect of ZrO_2 on the glass matrix in glass-ceramics. In addition, the ratio of (Ca+Sr) to Si is close to 1.0 for both glass#2ZrO_2 and glass#8ZrO_2, indicating the similar residual glass in glass-ceramics in present work. Therefore, the increase in conductivity of glass-ceramics can be mainly attributed to the increasing $(Ca,Sr)ZrO_3$ phase. It is also worth noting that the conductivity of glasses and glass-ceramics at 750 ºC ranges from 2.0×10^{-8} $S\cdot cm^{-1}$ to 8.5×10^{-7} $S\cdot cm^{-1}$, meeting the insulating requirement of sealing glasses ($<10^{-4}$ $S\cdot cm^{-1}$) for SOFCs application.[56]

3.3 Interfacial reaction

Fig. 4a shows the fraction of Cr^{6+} in the reaction couples between Cr_2O_3 and the glass powders after they have reacted in air at 700 ºC for different times. It is clear that the fraction of Cr^{6+} in the reaction couple decreases with increasing ZrO_2 content. Considering the amorphous nature of all species (in Fig. 2a), the improved chemical compatibility of the glasses at 700 ºC can be attributed to the condensed glass structure (in Fig. 1 and Table 2).

The fraction of Cr^{6+} in the reaction couples at 750 and 800 ºC increases with increasing ZrO_2 content, as shown in Figs. 4b and 4c. Our previous work showed that the chemical compatibility of a CaO-SrO-B_2O_3-SiO_2 sealing system can be improved by controlled crystallization of a Sr-containing phase. Thermodynamic calculation has also revealed that the Sr^{2+} ions in the crystalline phase (*e.g.*, Sr_2SiO_4) are more stable than their analogues in the glass matrix.[43, 49, 57, 58] Therefore, a greater amount of

RSC Advances Accepted Manuscript

residual glass weakens the chemical compatibility of the sealing glasses at 750 and 800 ºC.

Fig. 5 shows SEM micrographs of sealing couples held at 800 ºC for 500 hours and EDS line scans across the respective interfaces. Representative micrographs of glass#2ZrO_2 and glass#8ZrO_2 are chosen for comparison, as shown in Figs. 5a and 5b. The compositions of the selected spots in the glass-ceramics determined by EDS are summarized in Table 3. The results have been normalized for O content. Considerable amount of Sr and Ca can be detected in the Zr-enrichment zones (point#2 in Fig.5a, point#4 and point#5 in Fig.5b), as shown in Table 3. Therefore, one can deduce the presence of phases containing Ca, Sr and Zr according to EDS results. Based on XRD and EDS results (in Fig.2 and Fig.5), one can confirm the existence of the exact $(Ca_{0.612}Sr_{0.338})ZrO_3$ phase in present work.

In addition, good bonding can be observed at the interfaces between the Crofer 22APU and ZrO_2-containing glasses. Moreover, the EDS line scan reveals that the width of the reaction zones (enriched in Sr and Cr) at the glass/metal interfaces is ~2 μm, which is much thinner than the previous results under similar condition (5-30μm) in literature.[36] This indicates that the addition of ZrO_2 significantly improves the chemical compatibility of sealing glasses in present work.

4. Conclusions

The relationship between the structures and properties of ZrO_2-containing sealing glasses has been systematically investigated in present work. The addition of ZrO_2 strengthens the glass network, and thus, reduces the tendency of the glasses to crystallize. The CTE and electrical conductivity of glasses also decrease with increasing ZrO_2 content due to the condensed glass network. The CTE of glass-ceramics decreases with the addition of ZrO_2 because of the facilitated

RSC Advances Accepted Manuscript

crystallization of a low CTE phase ($CaSiO_3$); whereas, the electrical conductivity of glass-ceramics increases with ZrO_2 dopant due to the accelerated crystallization of $(Ca_{0.612}Sr_{0.388})ZrO_3$. The condensed glass network also reduces the interfacial reaction, whereas the greater amount of residual glass in glass-ceramics with ZrO_2 dopants favors the reaction. Moreover, a reaction zone of ~2 μm thick can be observed at the interface between ZrO_2-containing sealing glasses and Crofer 22APU held at 800 ºC for 500 hours. These findings on the structure-property correlation of sealing glass will be useful for the design of stable sealing glasses for SOFC applications.

Acknowledgments

The authors gratefully acknowledge the financial support of the National Natural Science Foundation of China (No. 51102045), Program for New Century Excellent Talents in Fujian Province University (No. JA12013), and the Undergraduate Innovative Experiment Program of Fujian Province (No. 201313470020). They would also like to thank Zhenhuan Zheng for assistance with SEM/EDS, Qingming Huang for assistance with X-ray diffraction, Fen Lin for assistance with DSC analysis, and Yunlong Yu for assistance with dilatometric measurement.

References

1. M.K. Mahapatra, K. Lu, *Journal of Power Sources*, 2010, **195**, 7129-7139.

2. K.S. Weil, *Sealing Technology for Solid Oxide Fuel Cells, in: Fuel Cell Science and Engineering*, Wiley-VCH Verlag GmbH & Co. KGaA, 2012, p. 301-333.

3. S.B. Sohn, S.Y. Choi, G.H. Kim, H.S. Song, G.D. Kim, *Journal of Non-Crystalline Solids*, 2002, **297**, 103-112.

4. M. Yano, A. Tomita, M. Sano, T. Hibino, *Solid State Ionics*, 2007, **177**, 3351-3359.

5. Y.S. Chou, J.W. Stevenson, G.G. Xia, Z.G. Yang, *Journal of Power Sources*, 2010,

RSC Advances Accepted Manuscript

95, 5666-5673.

6. S. Petrescu, M. Constantinescu, E.M. Anghel, I. Atkinson, M. Olteanu, M. Zaharescu, *Journal of Non-Crystalline Solids*, 2012, **358**, 3280-3288.

7. S. Ghosh, A.D. Sharma, A.K. Mukhopadhyay, P. Kundu, R.N. Basu, *International Journal of Hydrogen Energy*, 2010, **35**, 272-283.

8. T. Jin, K. Lu, *Journal of Power Sources*, 2010, **195**, 195-203.

9. T. Zhang, Q. Zou, *Journal of the European Ceramic Society*, 2012, **32**, 4009-4013.

10. A.A. Reddy, D.U. Tulyaganov, M.J. Pascual, V.V. Kharton, E.V. Tsipis, V.A. Kolotygin, J.M.F. Ferreira, *International Journal of Hydrogen Energy*, 2013, **38**, 3073-3086.

11. A. Shyam, R. Trejo, D. McClurg, A. Ladouceur, M. Kirkham, X. Song, J. Howe, E. Lara-Curzio, *Journal of Materials Science*, 2013, **48**, 5880-5898.

12. J. Wu, Z. Li, Y. Huang, F. Li, *Ceramics International*, 2013, **39**, 7743-7750.

13. A. Goel, D.U. Tulyaganov, A.M. Ferrari, E.R. Shaaban, A. Prange, F. Bondioli, J.M.F. Ferreira, *Journal of the American Ceramic Society*, 2010, **93**, 830-837.

14. S.T. Reis, M.J. Pascual, R.K. Brow, C.S. Ray, T. Zhang, *Journal of Non-Crystalline Solids*, 2010, **356**, 3009-3012.

15. M.K. Mahapatra, K. Lu, *Materials Science and Engineering: R: Reports*, 2010, **67**, 65-85.

16. D.U. Tulyaganov, A.A. Reddy, V.V. Kharton, J.M.F. Ferreira, *Journal of Power Sources*, 2013, **242**, 486-502.

RSC Advances Accepted Manuscript

17. S.J. Widgeon, E.L. Corral, M.N. Spilde, R.E. Loehman, *Journal of the American Ceramic Society*, 2009, **92**, 781-786.

18. N. Lahl, D. Bahadur, K. Singh, L. Singheiser, K. Hilpert, *Journal of the Electrochemical Society*, 2002, **149**, A607-A614.

19. Z. Yang, J.W. Stevenson, K.D. Meinhardt, *Solid State Ionics*, 2003, **160**, 213-225.

20. V. Kumar, G. Kaur, K. Lu, G. Pickrell, *International Journal of Hydrogen Energy*, 2015, **40**, 1195-1202.

21. G. Kaur, K. Singh, O.P. Pandey, D. Homa, B. Scott, G. Pickrell, *Journal of Power Sources*, 2013, **240**, 458-470.

22. Z. Yang, K.D. Meinhardt, J.W. Stevenson, *Journal of the Electrochemical Society*, 2003, **150**, A1095-A1101.

23. J.W. Fergus, *Journal of Power Sources*, 2005, **147**, 46-57.

24. Y.S. Chou, J.W. Stevenson, P. Singh, *Journal of Power Sources*, 2008, **184**, 238-244.

25. Y.S. Chou, J.W. Stevenson, P. Singh, *Journal of Power Sources*, 2008, **185**, 1001-1008.

26. G. Cabouro, G. Caboche, S. Chevalier, P. Piccardo, *Journal of Power Sources*, 2006, **156**, 39-44.

27. A. Ananthanarayanan, L. Montagne, B. Revel, G.P. Kothiyal, *AIP Conference Proceedings*, 2010, **1313**, 370-372.

28. F. Smeacetto, M. Salvo, F.D. D'Hérin Bytner, P. Leone, M. Ferraris, *Journal of the European Ceramic Society*, 2010, **30**, 933-940.

RSC Advances Accepted Manuscript

29. F. Smeacetto, M. Salvo, P. Leone, M. Santarelli, M. Ferraris, *Materials Letters*, 2011, **65**, 1048-1052.

30. F. Smeacetto, A. Chrysanthou, M. Salvo, T. Moskalewicz, F. D'Herin Bytner, L.C. Ajitdoss, M. Ferraris, *International Journal of Hydrogen Energy*, 2011, **36**, 11895-11903.

31. I.W. Donald, P.M. Mallinson, B.L. Metcalfe, L.A. Gerrard, J.A. Fernie, *Journal of Materials Science*, 2011, **46**, 1975-2000.

32. Y.S. Chou, E.C. Thomsen, R.T. Williams, J.P. Choi, N.L. Canfield, J.F. Bonnett, J.W. Stevenson, A. Shyam, E. Lara-Curzio, *Journal of Power Sources*, 2011, **196**, 2709-2716.

33. G. Kaur, O.P. Pandey, K. Singh, *International Journal of Hydrogen Energy*, 2012, **37**, 3883-3889.

34. T. Zhang, H. Zhang, G. Li, H. Yung, *Journal of Power Sources*, 2010, **195**, 6795-6797.

35. D. Saritha, Y. Markandeya, M. Salagram, M. Vithal, A.K. Singh, G. Bhikshamaiah, *Journal of Non-Crystalline Solids*, 2008, **354**, 5573-5579.

36. K. Sharma, G.P. Kothiyal, L. Montagne, F.O. Me´ar, B. Revel, *International Journal of Hydrogen Energy*, 2012, **37**, 11360-11369.

37. F. Smeacetto, M. Salvo, M. Ferraris, V. Casalegno, P. Asinari, *Journal of the European Ceramic Society*, 2008, **28**, 611-616.

38. B. Kaur, K. Singh, O.P. Pandey, *International Journal of Hydrogen Energy*, 2012, **37**, 3839-3847.

RSC Advances Accepted Manuscript

39. A.A. Reddy, D.U. Tulyaganov, A. Goel, M. Sardo, P.V. Wiper, M.J. Pascual, V.V. Kharton, V.A. Kolotygin, E.V. Tsipis, L. Mafra, J.M.F. Ferreira, J*ournal of Materials Chemistry A*, 2013, **1**, 6471-6480.

40. Y.Q. Shao, Z.Y. Yi, C. He, J.Q. Zhu, D. Tang, *Journal of American Ceramic Society*, 2015, **1**, 1-8.

41. Y.Y. Chen, T. Zhang, X. Wang, Y.Q. Shao, D. Tang, *Journal of American Ceramic Society*, 2008, **91**, 4154-4157.

42. T. Zhang, R.K. Brow, W.G. Fahrenholtz, S.T. Reis, *Journal of Power Sources*, 2013, **205**, 301-306.

43. T. Zhang, Q. Zou, F. Zeng, S. Wang, D. Tang, H. Yang, *Journal of Power Sources*, 2012, **216**, 1-4.

44. M.K. Mahapatra, K. Lu, *Journal of Materials Science*, 2009, **44**, 5569-5578.

45. G. Kaur, O.P. Pandey, K. Singh, *International Journal of Hydrogen Energy*, 2012, **37**, 6862-6874.

46. A. Goel, D.U. Tulyaganov, M.J. Pascual, E.R. Shaaban, F. Muñoz, Z. Lü, J.M.F. Ferreira, *Journal of Non-Crystalline Solids*, 2010, **356**, 1070-1080.

47. C.C. Lin, P. Shen, H.M. Chang, Y.J. Yang, *Journal of the European Ceramic Society*, 2006, **26**, 3613-3620.

48. A.M. Raul, F. Cuevas, O. Alves, N. Aranha, J.A. Sanjurjo, C. Cesar, L. Barbosa, *Journal of Materials Chemistry*, 1996, **6**, 1811-1814.

49. J.L. Chen, H. Yang, R. Chadeyron, D. Tang, T. Zhang, *Journal of the European Ceramic Society*, 2014, **34**, 1989-1996.

RSC Advances Accepted Manuscript

50. D.A. McKeown, I.S. Muller, A.C. Buechele, I.L. Pegg, C.A. Kendziora, *Journal of Non-Crystalline Solids*, 2000, **262**, 126-134.

51. P.P. Bihuniak, R.A. Condrate, *Journal of Non-Crystalline Solids*, 1981, **44**, 331-343.

52. S.F. Song, Z.Y. Wen, Y. Liu, Q.X. Zhang, X.W. Wu, J.C. Zhang, J.D. Han, *Ceramics International*, 2009, **35**, 3037-3042.

53. H. Li, Y.L. Su, L.Y. Li, D.M. Strachan, *Journal of Non-Crystalline Solids*, 2001, **292**, 167-176.

54. K.S. Weil, J. Deibler, J. Hardy, L.A. Chick, C. Coyle, D. Kim, G.G. Xia, *Journal of Materials Engineering and Performance*, 2004, **13**, 316-326.

55. S.C. Hwang, G.M. Choi, *Journal of the European Ceramic Society*, 2005, **25**, 2609–2612.

56. P. Lessing, *Journal of Materials Science*, 2007, **42**, 3465-3476.

57. J.L. Chen, Q. Zou, F.R. Zeng, S.R. Wang, D. Tang, H.W. Yang, T. Zhang, *Journal of Power Sources*, 2013, **241**, 578-582.

58. S.R. Chen, J.X. Lin, H.W. Yang, D. Tang, T. Zhang, *Journal of Power Sources*, 2014, **267**, 753-759.

RSC Advances Accepted Manuscript

List of tables

Table 1 Batch composition (in mol. %) of sealing glasses.

Table 2 Thermal properties of sealing glasses and glass-ceramics.

Table 3 EDS results for selected spots in Fig. 5 (in at. %). The results have been normalized for O content.

Table 1 Batch composition (in mol. %) of sealing glasses.

Sample ID	SrO	CaO	B_2O_3	SiO_2	ZrO_2
glass#2ZrO_2	25.48	25.48	7.84	39.20	2.00
glass#4ZrO_2	24.96	24.96	7.68	38.40	4.00
glass#6ZrO_2	24.44	24.44	7.52	37.60	6.00
glass#8ZrO_2	23.92	23.92	7.36	36.80	8.00

Table 2 Thermal properties of sealing glasses and glass-ceramics.

Sample ID	Glass#2ZrO_2	Glass#4ZrO_2	Glass#6ZrO_2	Glass#8ZrO_2
Thermal parameters				
T_g (ºC)	685±3	705±3	713±3	726±3
T_d (ºC)	748±3	752±3	779±3	787±3
T_x (ºC)	869±3	909±3	894±3	901±3
Density ($g \cdot cm^{-3}$)	3.40±0.02	3.44±0.02	3.48±0.02	3.53±0.02
CTE ($\times 10^{-6}$ K^{-1}, 200-600 ºC)				
glasses	12.6±0.1	13.1±0.1	12.1±0.1	12.4±0.1
800 ºC for 500 hours	12.2±0.1	12.2±0.1	11.1±0.1	10.5±0.1
Crystalline content (weight %)				
800 ºC for 2 hours	71±5	67±5	65±5	60±5

T_g: glass transition temperature
T_d: softening temperature
T_x: onset crystallization temperature
CTE: coefficient of thermal expansion

RSC Advances Accepted Manuscript

Table 3 EDS results for selected spots in Fig. 5 (in at. %). The results have been normalized for O content.

Spot	**1**	**2**	**3**	**4**	**5**
Sr	27	40	25	38	21
Ca	22	10	25	10	26
Si	51	3	50	0	40
Zr	0	47	0	52	14

RSC Advances Accepted Manuscript

List of figures

Fig. 1 MAS NMR spectra of glasses for (a) ^{11}B and (b) ^{29}Si.

Fig. 2 XRD patterns of glass-ceramics held at (a) 700 ºC for 5 hours, (b) 800 ºC for 2 hours and (c) 800 ºC for 500 hours. (d) The patterns of Fig.2c plotted in the 2θ range of 20-35°.

Fig. 3 The temperature dependence of conductivity (log σ versus 1000 T^{-1}) for glasses and glass-ceramics, measured in air from 650 to 750 ºC.

Fig. 4 Fraction of Cr^{6+} in the reaction couples between Cr_2O_3 and glass powders after they have reacted in air for different times at (a) 700 ºC, (b) 750 ºC, and (c) 800 ºC .

Fig. 5 Micrographs of glass-metal interfaces held at 800 ºC for 500 hours and EDS elemental line scans across the respective interfaces for (a) glass#2ZrO_2 and (b) glass#8ZrO_2.

RSC Advances Accepted Manuscript

Fig. 1

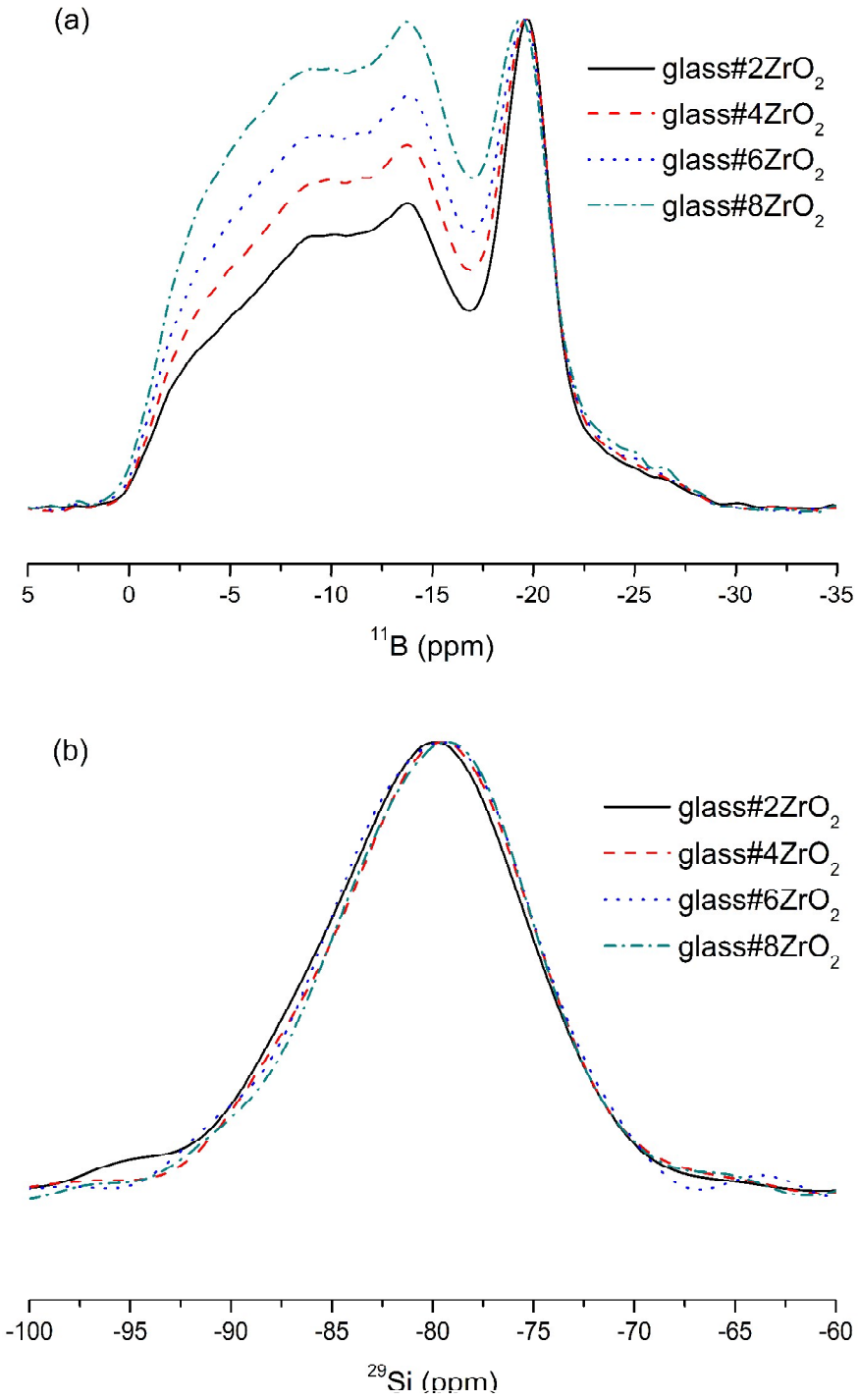

Fig. 1 MAS NMR spectra of glasses for (a) ^{11}B and (b) ^{29}Si.

RSC Advances Accepted Manuscript

Fig. 2

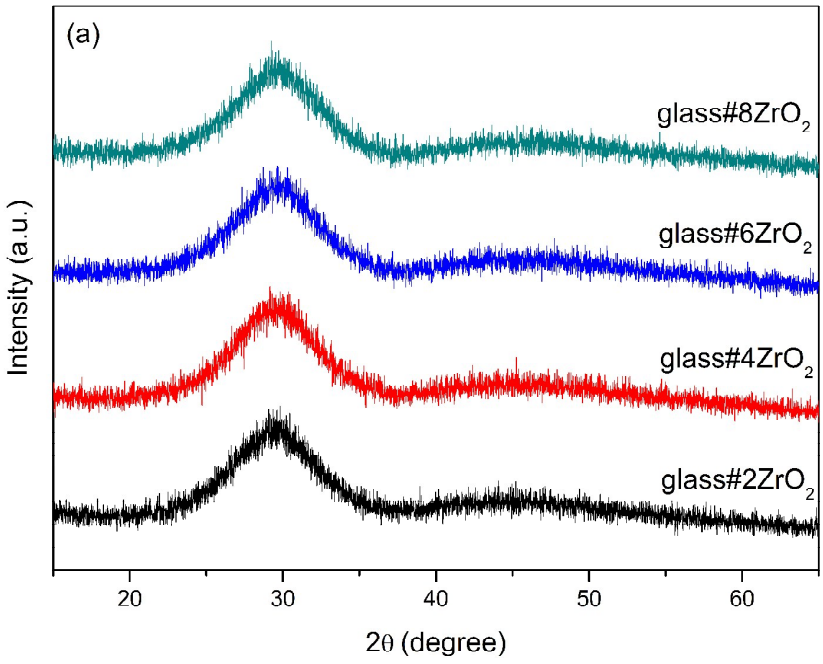

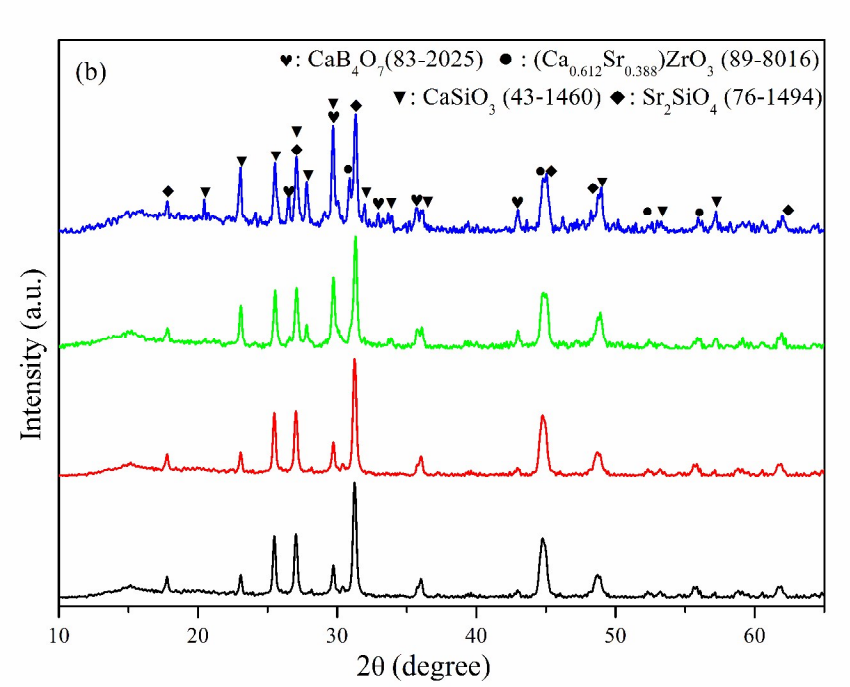

RSC Advances Accepted Manuscript

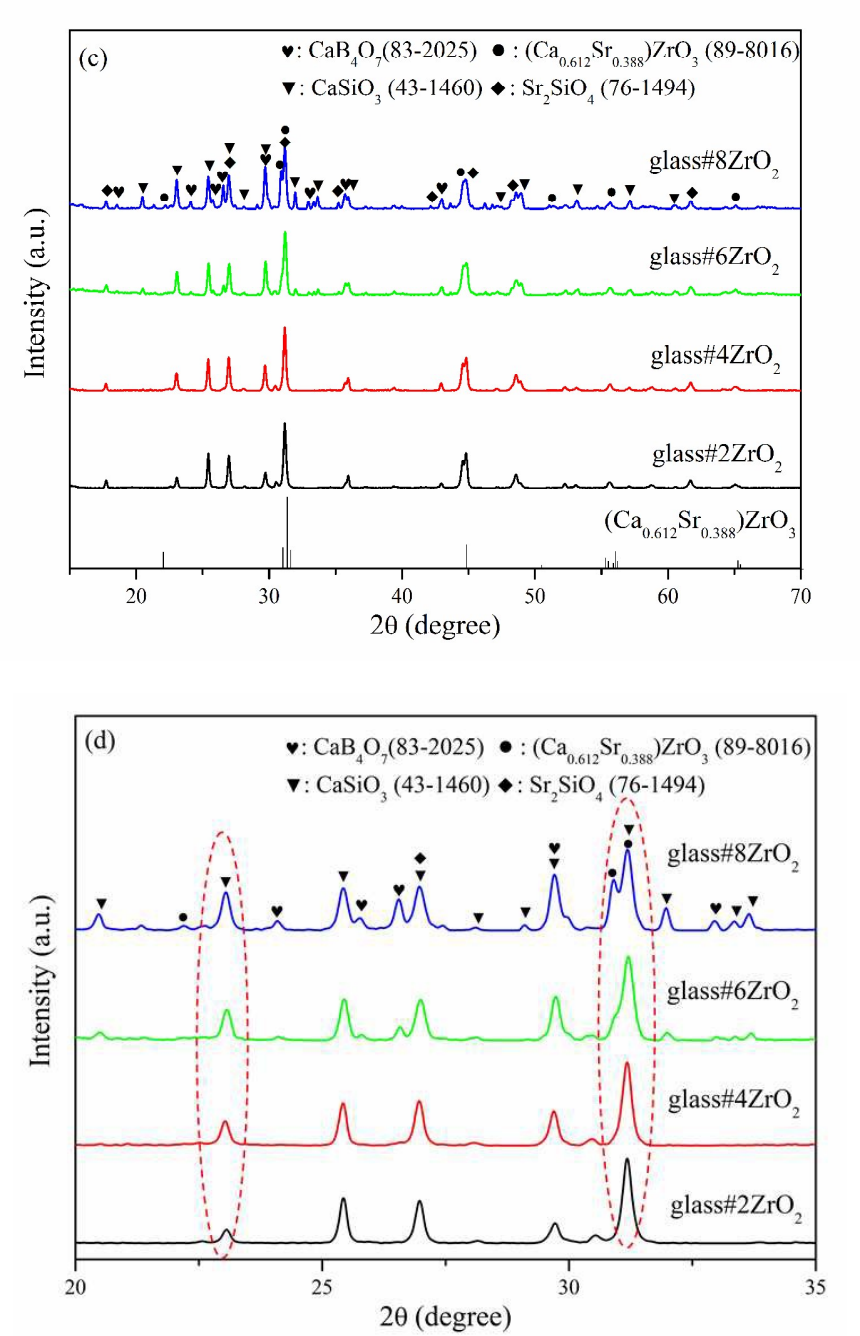

Fig. 2 XRD patterns of glass-ceramics held at (a) 700 ºC for 5 hours, (b) 800 ºC for 2 hours and (c) 800 ºC for 500 hours. (d) The patterns of Fig.2c plotted in the 2θ range of 20-35°.

RSC Advances Accepted Manuscript

Fig. 3

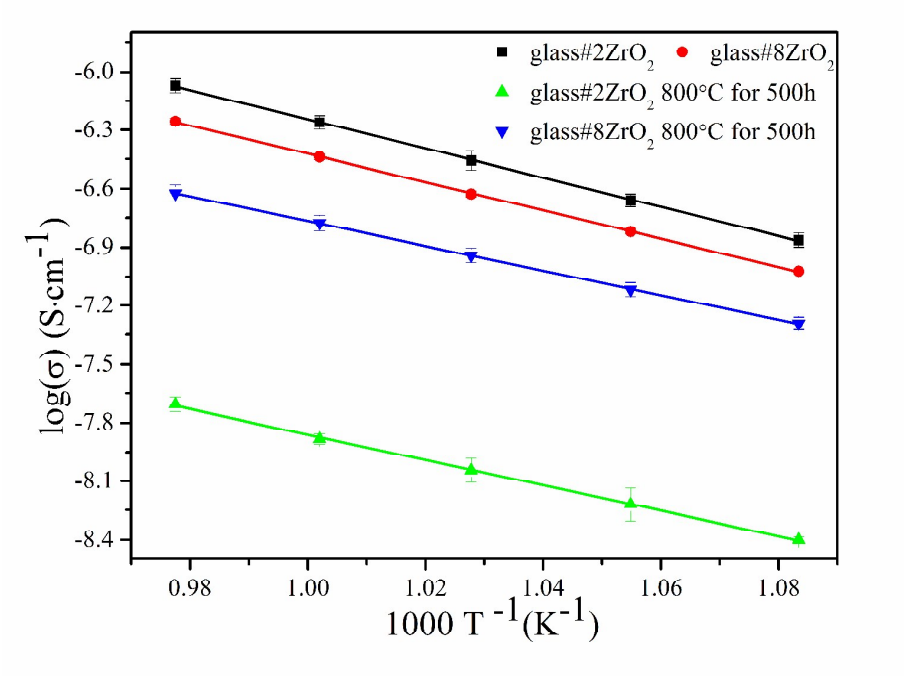

Fig. 3 The temperature dependence of conductivity (log σ versus 1000 T^{-1}) for glasses and glass-ceramics, measured in air from 650 to 750 ºC.

RSC Advances Accepted Manuscript

Fig. 4

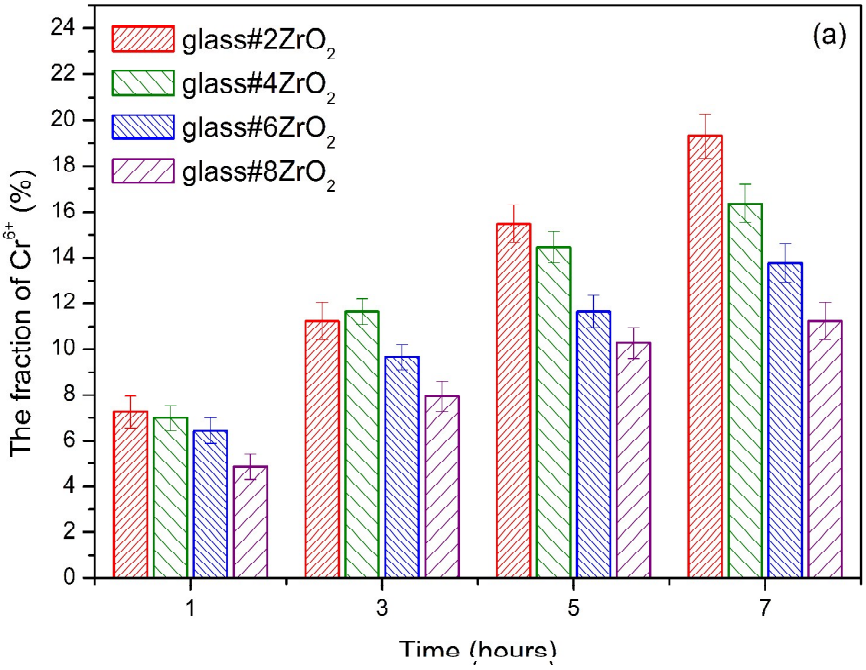

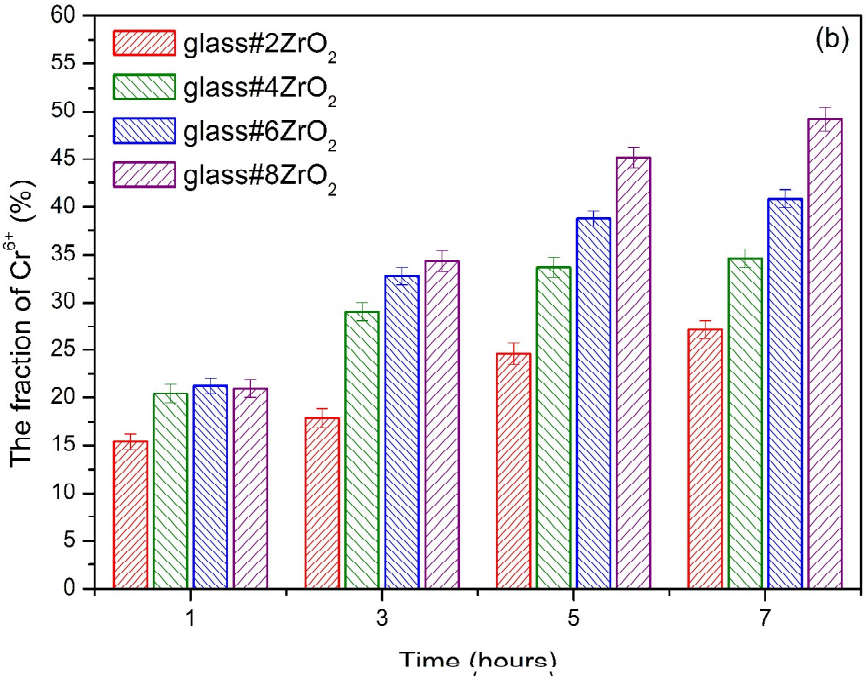

RSC Advances Accepted Manuscript

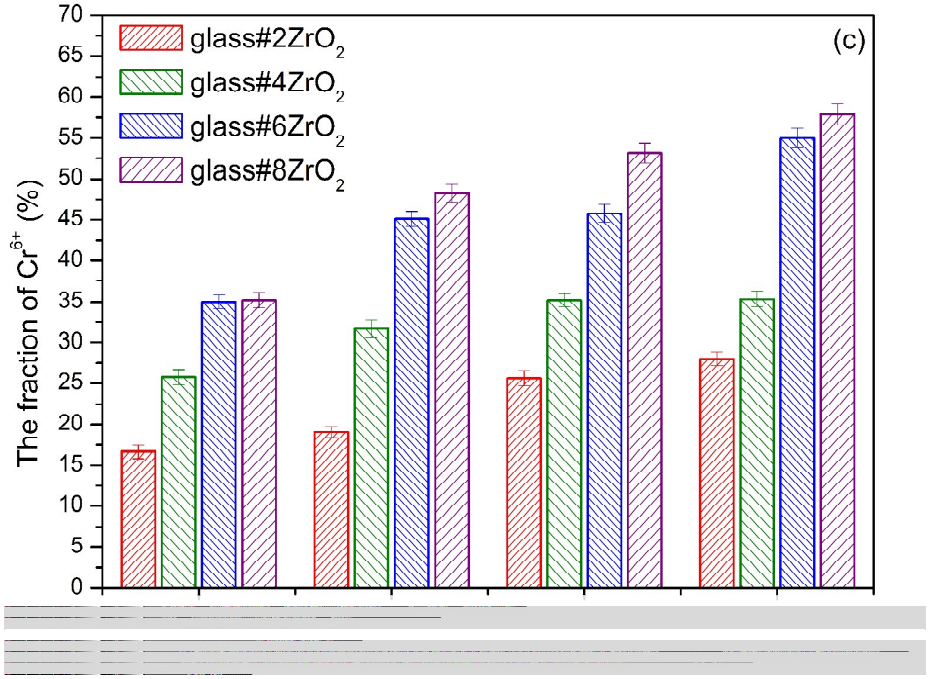

Fig. 4 Fraction of Cr^{6+} in the reaction couples between Cr_2O_3 and glass powders after they have reacted in air for different times at (a) 700 ºC, (b) 750 ºC, and (c) 800 ºC .

RSC Advances Accepted Manuscript

Fig. 5

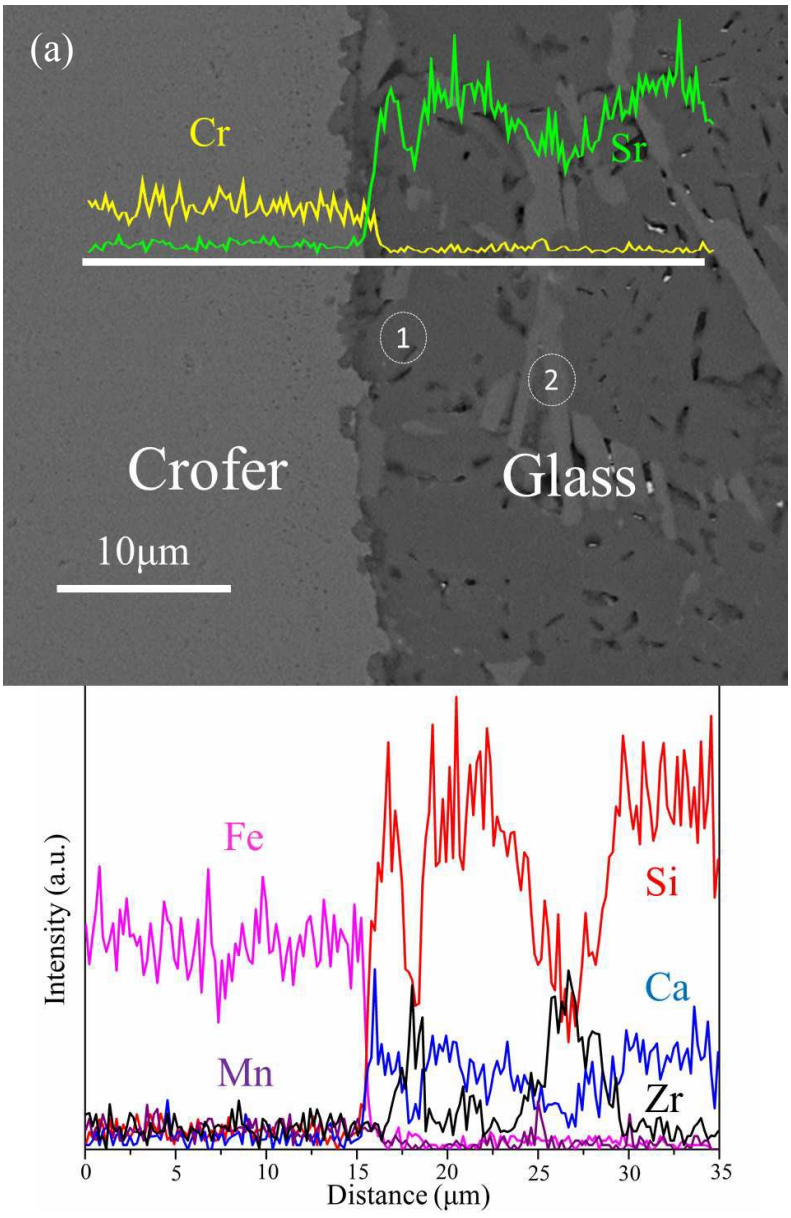

RSC Advances Accepted Manuscript

Fig. 5

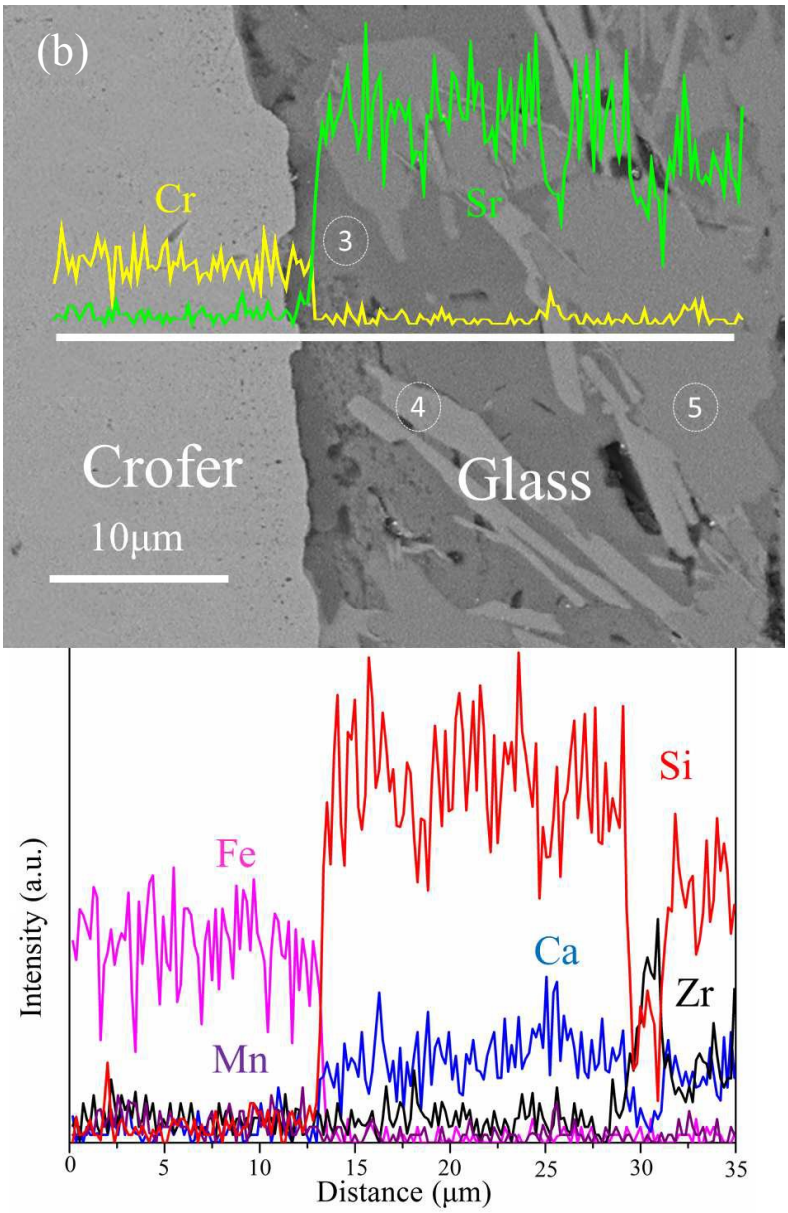

Fig. 5 Micrographs of glass-metal interfaces held at 800 ºC for 500 hours and EDS elemental line scans across the respective interfaces for (a) glass#2ZrO_2 and (b) glass#8ZrO_2.

RSC Advances Accepted Manuscript